MS-GDUN:Multi-Scale Graph Deep Unfolding Network with Gradient-Threshold Learning for FMT Reconstruction

Xiaowei He[1], Chunyu Qiu[1,2], Xin Zhao[1], Liuyuan Zhang[1], Xuelei He[1], and Hongbo Guo[1*]

[1] School of Information Sciences and Technology, Northwest University, Xi'an, 710127, China
[2] School of Network and Data Center, Northwest University, Xi'an, 710127, China
Guohb@nwu.edu.cn

Abstract. Fluorescence Molecular Tomography (FMT) enables non-invasive quantification of early-stage tumors, but its clinical utility is hampered by the severe ill-posedness of its inverse reconstruction problem. Traditional iterative methods rely on proximal gradient descent and soft-thresholding for non-convex sparse optimization, yet suffer from poor stability under strong noise and tissue scattering—attributed to their sensitivity to hand-crafted parameters, gradient approximation errors, and rigid fixed global sparsity thresholds. To address these limitations, we propose the Multi-Scale Graph Deep Unfolding Network with Gradient-Threshold Learning (MS-GDUN), a physics-guided deep unfolding framework that synergizes iterative reconstruction logic with graph neural networks. MS-GDUN unfolds classical iterative pipelines into a layered learnable architecture, enabling end-to-end joint learning of iteration-specific gradient update directions and node-adaptive sparsity thresholds in place of manual parameter tuning. We construct physics-constrained graphs via finite-element mesh photon transport distances, use Graph Convolutional Blocks (GCB) to model multi-hop photon diffusion correlations, and introduce a Multi-Scale Graph Cross-Attention (MSGC) mechanism to fuse local-global features across four scales, mitigating single-scale limitations and enhancing reconstruction structural consistency. Extensive experiments on simulated and clinical datasets validate that MS-GDUN outperforms state-of-the-art conventional iterative and learning-based methods in tumor localization accuracy and morphological fidelity. This work establishes MS-GDUN as a robust, reliable FMT reconstruction paradigm with great potential for early tumor detection. Code is available at `https://github.com/LeTeddy/MS-GDUN`.

Keywords: Fluorescence molecular tomography · Multi-Scale Graph Deep Unfolding Network · Learnable Gradient-Threshold.

* Corresponding author.

1 Introduction

Fluorescence Molecular Tomography (FMT) is a noninvasive three dimensional imaging modality capable of detecting in-vivo tissues and pharmaceutical agents, offering notable advantages such as low cost, high sensitivity, and strong specificity [17, 4]. This technique exhibits substantial potential in applications including early tumor diagnosis and drug development [20, 14], serving as a key modality in the evolution of whole-body photonic imaging [15]. However, owing to strong photon scattering, sparse source configurations, and limited surface measurement data, the associated inverse reconstruction problem remains severely ill-posed.

Given the sparsity characteristics of the FMT inverse problem, numerous regularization based reconstruction algorithms have been proposed [25, 3, 7, 22]. Classical L_2-norm methods such as Tikhonov regularization tend to introduce over-smoothing, whereas L_1-norm regularization and Sparse Graph Manifold Learning (SGML), solved via the Iteratively Reweighted Soft-Thresholding Algorithm (IRSTA) [6], have been adopted to enhance sparsity and incorporate three dimensional structural priors. However, these methods are generally built upon simplified approximations of the Radiative Transfer Equation (RTE), leading to modeling errors, and their reliance on empirical parameter tuning increases computational cost and limits performance.

Compared with traditional iterative algorithms, deep learning has demonstrated significant advantages in solving imaging inverse problems by learning non-iterative mappings from large-scale datasets, thereby alleviating modeling errors induced by simplified light propagation models and improving reconstruction accuracy [10]. Representative approaches include based on MLP end to end networks, UHR-DeepFMT, and three dimensional encoder decoder architectures [5, 24, 8]; however, these data driven methods often suffer from limited generalization and insufficient exploitation of three dimensional topological information in FMT. To address these limitations, Deep Unrolling Networks (DUNs) [13], such as ADMM-CSNet and ISTA-Net, improve interpretability and generalization by mimicking traditional iterative update schemes [21, 23]. In addition, although Graph Convolutional Networks (GCNs) are well suited for FMT reconstruction due to the finite element mesh structure [2, 9, 19], existing GCN-based methods neglect distance-related structural correlations and exhibit high computational cost and training instability under extremely sparse source configurations—a setting that also induces severe node-level class imbalance [12, 26], which limits stable high-accuracy reconstruction.

To address challenges like insufficient structural similarity under sparse sources, multi source resolution limits, and gradient vanishing in FMT reconstruction, we propose the Multi-Scale Graph Deep Unfolding Network with Gradient-Threshold Learning (MS-GDUN). By unfolding Sparse Graph Manifold Learning (SGML) process into a learnable architecture, we achieve highly accurate tomographic reconstruction. Our main contributions are threefold: 1) First, integrating physics informed global context modeling and customized transfer learning to capture structural dependencies, enhancing localization accuracy and shape

fidelity. 2) Second, designing node adaptive sparsity with gradient threshold learning to mitigate gradient vanishing and preserve high resolution in multi source settings. 3) Third, proposing multi scale graph feature aggregation with cross-attention to overcome single scale limitations, enabling robust representation of structural details. Extensive experiments demonstrate that MS-GDUN outperforms existing methods, promising to advance FMT's preclinical and clinical translation in early tumor detection.

2 Method

Based on photon propagation theory and the finite element method (FEM), fluorescence molecular tomography can be formulated as a linear inverse problem with graph-structured regularization [16, 18, 11]. The SGML model introduces a graph-based manifold regularization to enforce spatial consistency of the source distribution on the finite-element mesh. The optimization problem is formulated as:

$$\min_X \ \frac{1}{2}\|MX - b\|_2^2 + \lambda\|LX\|_2^2 + \zeta\|X\|_p \tag{1}$$

where M denotes the photon propagation system matrix, X is the unknown in vivo fluorescence source distribution, and b represents the measured surface photon flux. λ and ζ are regularization parameters. The Laplacian matrix L encodes the mesh topology and is dynamically updated during the iterative reconstruction to adapt to the evolving source distribution.

The SGML model is traditionally solved using IRSTA. At each iteration, by applying a proximal gradient descent approach to the smooth term $f(X) = \frac{1}{2}\|MX - b\|_2^2 + \lambda\|L_{k+1}X\|_2^2$ and converting the non-convex sparse term into a soft-thresholding problem, the closed-form solution for the update X_{k+1} can be expressed as:

$$\hat{X_k} = X_k - \frac{1}{\nabla^2 f(X_k)}\nabla f(X_k) \tag{2}$$

$$X_{k+1} = soft(\hat{X_k}, \frac{\zeta}{\nabla^2 f(X_k)}) \tag{3}$$

where $soft(\cdot)$ is the soft-threshold function, and the threshold is $\frac{\zeta}{\nabla^2 f(X_k)}$. ζ is a manually set parameter. First-order derivative $\nabla f(X)$ represents the gradient descent direction at each iteration, while the second-order derivative $\nabla^2 f(X)$ determines the step size through its inverse $\frac{1}{\nabla^2 f(X)}$ in the gradient descent update, respectively:

$$\begin{cases} \nabla f(X_k) = M^T M X_k - M^T \phi + 2\zeta L_{k+1}^T L_{k+1} X_k \\ \nabla^2 f(X_k) = M^T M + 2\zeta L_{k+1}^T L_{k+1} \end{cases} \tag{4}$$

2.1 MS-GDUN Network Architecture Design

MS-GDUN is a physics-guided deep unfolding network derived from the SGML-IRSTA solver, as shown in Fig. 1. By unfolding the iterative updates in Eqs. 2-3

into $N = 6$ stages (selected via ablation over $N \in [4, 10]$), each stage preserves the original optimization structure while replacing analytical quantities with learnable modules. The network learns the gradient term $\nabla f(X_k)$ and the adaptive threshold $\frac{\zeta}{\nabla^2 f(X_k)}$ in a data-driven manner. The learned gradient is used to perform the update in Eq. 2, and the learned threshold is used in Eq. 3. Thus MS-GDUN maintains the interpretability of SGML-IRSTA while enabling iteration-dependent, learnable optimization.

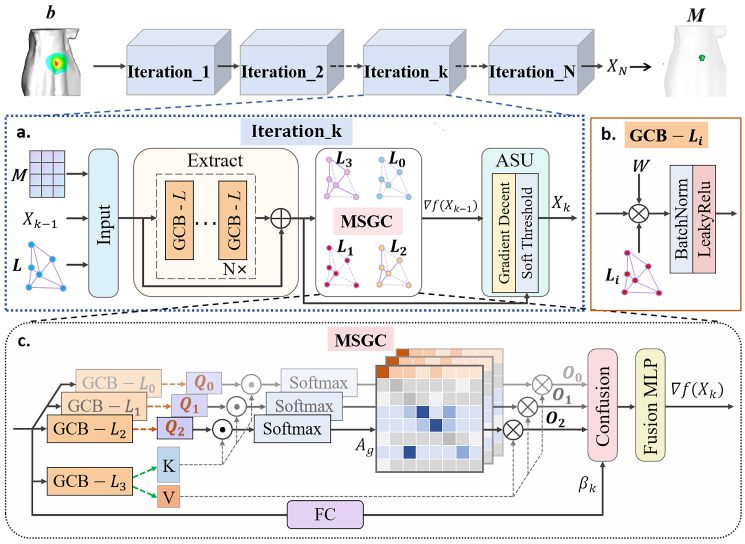

Fig. 1. Overall framework of MS-GDUN. (a) Unfolded iterative pipeline at the k-th stage; (b) Basic graph convolutional block parameterized by the Laplacian matrix L_i; (c) Multi-scale graph convolution module with cross-attention, which extracts and fuses multi-scale graph information to predict the iteration-dependent gradient for reconstruction.

At the k-th stage, the *Input Module* constructs physics-consistent features $X_{in} = [M^T M X_k,\ M^T b,\ L^T L X_k,\ X_k]$ which correspond to the analytical components of SGML-IRSTA. The *Feature Extract Module* maps X_{in} to topology-aware node representations F_k through graph convolutions defined on the finite-element mesh. Based on F_k, the *Multi-Scale Graph Convolutional Block* fuses multi-scale features via local KNN attention with sensitivity-weighted keys/values, and the *Adaptive Sparse Update* applies Softplus-predicted node-adaptive thresholds to suppress noise. These modules form a unified pipeline that enhances structural consistency.

2.2 Multi-scale Graph Feature Extraction and Fusion

To model structural dependencies at different spatial ranges, we introduce a set of pre-defined multi-scale Laplacian matrices $L_{multi} = \{L_0, L_1, L_2, L_3\}$ constructed with increasing neighborhood radii of 0.5, 1.0, and 1.5 mm on the finite-element mesh. At the k-th stage, graph convolutional blocks parameterized by L_0, L_1, and L_2 extract local structural features, while L_3 encodes global contextual information. Multi-scale features are fused through a graph cross-attention mechanism [1]:

$$Q_k^{(i)} = \mathcal{P}_{Q,k}^{i}(\mathcal{G}_{L_i}(F_k)), \quad K_k = \mathcal{P}_{K,k}(\mathcal{G}_{L_3}(F_k)), \quad V_k = \mathcal{P}_{V,k}(\mathcal{G}_{L_3}(F_k)) \tag{5}$$

where $\mathcal{G}_{L_i}(\cdot)$ denotes a graph convolutional block with Laplacian L_i, and $\mathcal{P}(\cdot)$ denotes a node-wise linear mapping.

Node-wise sensitivity weights derived from the forward matrix M are used to modulate key and value features:

$$s_i = \frac{\|M_{:,i}\|_2}{\max_j \|M_{:,j}\|_2}. \tag{6}$$

To control computational cost, attention is computed locally within neighborhood $\mathcal{N}_i$:

$$O_k^{(i)} = \mathit{Attention}(Q_k^{(i)}, \{s_j K_{k,j}\}_{j\in\mathcal{N}_i}, \{s_j V_{k,j}\}_{j\in\mathcal{N}_i}). \tag{7}$$

The outputs from different scales are fused to generate the learned gradient:

$$\nabla f(X_k) = \mathcal{P}\left(\sum_{i=0}^{2} \beta_{k,i} O_k^{(i)}\right), \tag{8}$$

where $\beta_{k,i}$ are learnable fusion weights.

2.3 Adaptive Sparse Update Strategy

At each unfolding stage, the reconstruction is updated as

$$X^k = \mathcal{S}_{\theta_k}\left(X^{k-1} - \alpha_k \nabla f(X_k)\right), \tag{9}$$

where α_k is a learnable diagonal preconditioner approximating the inverse Hessian, and $\mathcal{S}_{\theta_k}(\cdot)$ denotes a node-wise shrinkage operator.

The adaptive thresholds are predicted from graph features:

$$\theta_k = \mathrm{Softplus}(\mathcal{P}(F_k)), \quad \mathrm{Softplus}(x) = \ln(1 + e^x). \tag{10}$$

By jointly learning update directions and node-adaptive sparsity thresholds, MS-GDUN replaces the analytical gradient, fixed step size, and global threshold in SGML-IRSTA with data-driven, iteration-dependent optimization.

3 Experiments and Results

3.1 Data preparation and Compared methods

To evaluate the performance of the proposed MS-GDUN, both numerical simulations based on a digital mouse model and in-vivo experiments were conducted. In the numerical simulations, a virtual mouse anatomical model was constructed, including major organs such as muscle, heart, liver, stomach, kidney, and lungs, and discretized into a standard tetrahedral mesh consisting of 6,674 nodes and 33,357 tetrahedral elements. To generate training data, dual spherical fluorescent sources were randomly placed within the abdominal region of the virtual mouse, with a source radius ranging from $0.8 - 1.4mm$ and an edge-to-edge distance (EED) of $4 - 6mm$. Under 800 nm excitation and 1300 nm emission, surface fluorescence measurements were generated using the finite element method (FEM), producing a total of 29,368 samples.

To quantitatively evaluate the accuracy of MS-GDUN, we compared it with deep unfolding methods (ISTA-Net and FISTA-Net), a GCN-based approach (ResGCN), and a deep-learning reconstruction method (IPS). All models were trained on 80% of the data and tested on the remaining 20%, using the Dice similarity coefficient (Dice) and localization error (LE) as metrics. All models were implemented in PyTorch, trained with AdamW (initial learning rate 1×10^{-3}, batch size 8, 100 epochs) on a single RTX A6000 GPU.

3.2 Quantitative and Qualitative Results

Feasibility Experiments: To validate the feasibility of the proposed MS-GDUN, dual source experiments were conducted. Two spherical sources with a fixed radius of 1 mm were employed, and two groups of experiments were designed with EED of 4 mm and 6 mm, respectively, to investigate the model's resolution capability for closely spaced sources. Fig 2 presents a comparative visualization of the reconstruction results obtained by MS-GDUN and five competing methods from both two dimensional and three dimensional perspectives under different EED settings. Specifically, when the source separation was 4 mm, the IPS algorithm failed to effectively distinguish the two sources. Although FISTA-Net exhibited relatively good localization accuracy, it generated noticeable artifacts and showed poor structural similarity. Similarly, ResGCN performed unsatisfactorily at small source separations, likely due to overfitting caused by the lack of deep-unfolding-based generalization in graph convolution. In contrast, MS-GDUN achieved stable reconstruction across both separations. As shown in Table 1, MS-GDUN attained superior Dice scores, while the minimum LE was 0.002 mm. Notably, as the source separation decreased, MS-GDUN maintained stable reconstruction performance, further demonstrating its robustness and superiority over competing approaches.

Ablation Experiments: To investigate the impact of the multi scale graph cross attention mechanism and the adaptive sparse update strategy on feature

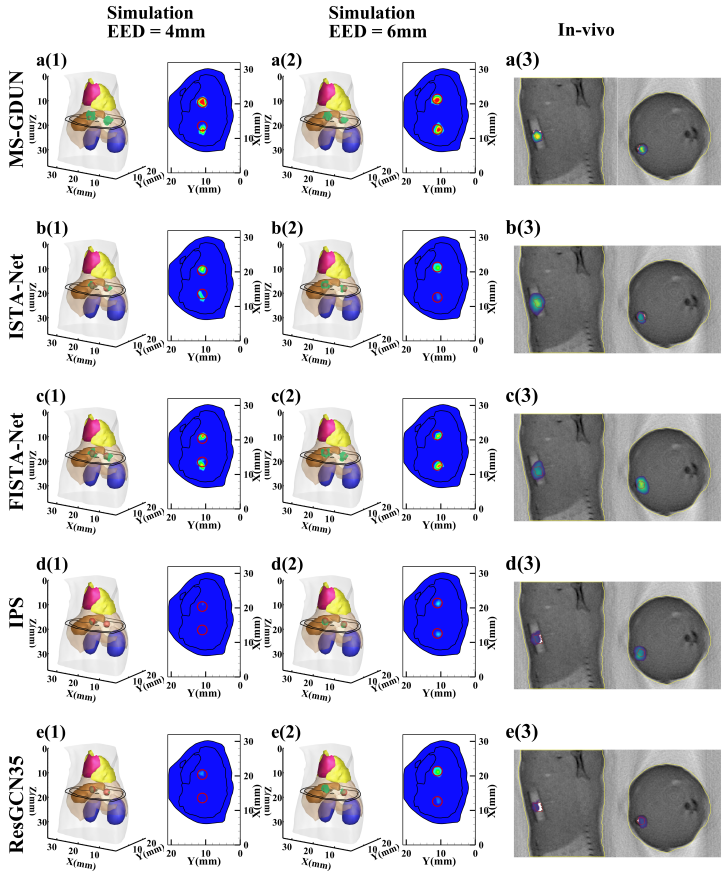

Fig. 2. Dual-source and in-vivo reconstruction results of five methods in 3D and transverse views. (a1–e1), (a2–e2), and (a3–e3) denote EED = 4 mm, EED = 6 mm, and in-vivo cases, respectively. Red circles indicate ground truth.

extraction in the proposed MS-GDUN, ablation studies were conducted. MS-GDUN represents the complete model. w/o GCB-L denotes the variant in which the multi scale graph convolution module is removed and all graph convolutions are replaced with a single scale configuration. w/o MSGC refers to the model without the graph cross attention mechanism, where multi scale output features are directly concatenated and fed into a linear layer. w/o ASUS denotes the model without the adaptive sparsification update strategy, in which all nodes are assigned an identical sparsity threshold. As shown in Table 2, removal of any component leads to performance degradation. The absence of MSGC and ASUS leads to degraded LE and Dice metrics. In addition, removing the GCB-L module results in a dramatic decrease in the Dice score to approximately 20%,

Table 1. Quantitative results of dual-source (simulation) and in-vivo reconstruction.

Experiment	Index	**MS-GDUN**	ResGCN	ISTA-Net	FISTA-Net	IPS
Sim,EED=4	LE (mm)	**0.002**	0.141	0.272	**0.124**	0.777
	Dice	**81.1%**	54.6%	**81.7%**	62.5%	39.9%
Sim, EED=6	LE (mm)	**0.078**	**0.016**	0.227	0.202	0.903
	Dice	**87.7%**	69.0%	**84.5%**	74.7%	54.6%
In-vivo	LE (mm)	**0.200**	0.298	0.268	0.349	**0.133**
	Dice	**54%**	28%	**41%**	25%	31%

Bold indicates best and second-best performance.

accompanied by a substantial deterioration in LE. These results demonstrate that GCB-L, MSGC, and ASUS play critical roles in the MS-GDUN framework.

Table 2. Ablation experimental results on the effectiveness of MS-GDUN.

Description	LE (mm) ↓	Dice ↑	MSE ↑
MS-GDUN	$\mathbf{0.068 \pm 0.009}$	$\mathbf{82.6 \pm 0.5\%}$	**0.0007**
w/o GCB-L	0.084 ± 0.011	$62.2 \pm 1.1\%$	0.0015
w/o MSGC	0.095 ± 0.015	$71.1 \pm 1.6\%$	0.0010
w/o ASUS	0.072 ± 0.008	$79.5 \pm 0.7\%$	0.0008

Computational Cost: MS-GDUN contains only 7,218 learnable parameters, independent of mesh size N_{node}. The multi-scale Laplacians are precomputed, fixed, and sparse—each node connects only to a small local neighborhood—yielding $O(N_{node})$ overall complexity. Training takes ∼1.2 h/epoch, and inference requires 80–150 ms per sample with 8–10 GB peak GPU memory.

In-Vivo Experiments: To comprehensively evaluate the reconstruction performance of MS-GDUN in a realistic biological environment, in-vivo experimental studies were conducted. In the in-vivo experiments, 6-8 week old female BALB/c nude mice were used to construct both luminescent source implantation models and orthotopic glioma models, with additional dual tube implantation experiments to evaluate the algorithm's multi source resolution. In the glioma model, approximately 1×10^6 U87 MG-GFP-FUC cells were injected into the mouse cerebral cortex. Subsequently, multi modal data including CT and MRI were acquired to perform 3D FMT reconstruction. All animal procedures strictly adhered to relevant institutional ethical guidelines and experimental regulations. The visualization results in Fig 2 indicate that the MS-GDUN method achieves superior spatial consistency in the reconstructed fluorescence regions, with shapes and boundary alignments that more closely match the true lesion. Table 1 presents the quantitative evaluation metrics of the reconstruction results, demonstrating that the MS-GDUN method achieves the highest Dice, thereby validating its effectiveness in real experimental settings.

4 Conclusion

In this study, we proposed MS-GDUN for robust fluorescence molecular tomography reconstruction. The framework combines physics-guided unfolding with multi-scale graph modeling and adaptive sparsification to improve stability and structural fidelity. Experimental results demonstrate that MS-GDUN outperforms existing iterative and learning-based methods in both simulations and in-vivo studies. Notably, it successfully distinguishes tumors with an edge-to-edge distance of 4 mm, achieving over 81% Dice and a minimum localization error of 0.002 mm, while maintaining stable performance under reduced source separation. In real biological experiments, it yields more accurate boundary alignment and competitive quantitative metrics. These results highlight its strong potential for reliable, high-resolution FMT reconstruction and early tumor detection.

Acknowledgments. This study was funded by the National Natural Science Foundation of China under Grants 12271434, 62271394, 62201459; the Scientific and Technological projects of Xi'an under Grant 201805060ZD11CG44; the Scientific and Technology New Star in Shaanxi Province of China under Grant 2023KJXX-035; General Project of the Key Research and Development Plan of Shaanxi Province under Grant 2025SF-YBXM-240; Natural Science Basic Research Plan in Shaanxi Province of China under Grant 2023-JC-JQ-57; Artificial intelligence empowers the team of "scientists + engineers" in education under 2024JH-KGDW-0084.

Disclosure of Interests. The authors have no conflicts to disclose.

References

1. Chen, C.F.R., Fan, Q., Panda, R.: Crossvit: Cross-attention multi-scale vision transformer for image classification. In: Proceedings of the IEEE/CVF international conference on computer vision. pp. 357–366 (2021)
2. Fabijańska, A., Banasiak, R.: Graph convolutional networks for enhanced resolution 3d electrical capacitance tomography image reconstruction. Applied Soft Computing **110**, 107608 (2021)
3. Feng, J., Qin, C., Jia, K., Zhu, S., Liu, K., Han, D., Yang, X., Gao, Q., Tian, J.: Total variation regularization for bioluminescence tomography with the split bregman method. Applied Optics **51**(19), 4501–4512 (2012)
4. Gaind, V., San, A.K., Lin, D., Webb, K.J.: Prediction of electric field frequency correlations for randomly scattering slabs in the nondiffusive regime with the scalar bethe–salpeter equation. Optics Letters **39**(1), 1–4 (2013)
5. Gao, Y., Wang, K., An, Y., Jiang, S., Meng, H., Tian, J.: Nonmodel-based bioluminescence tomography using a machine-learning reconstruction strategy. Optica **5**(11), 1451–1454 (2018)
6. Guo, H., Gao, L., Yu, J., He, X., Wang, H., Zheng, J., Yang, X.: Sparse-graph manifold learning method for bioluminescence tomography. Journal of biophotonics **13**(4), e201960218 (2020)
7. Guo, H., Yu, J., He, X., Hou, Y., Dong, F., Zhang, S.: Improved sparse reconstruction for fluorescence molecular tomography with l1/2 regularization. Biomedical optics express **6**(5), 1648–1664 (2015)

8. Guo, L., Liu, F., Cai, C., Liu, J., Zhang, G.: 3d deep encoder–decoder network for fluorescence molecular tomography. Optics letters **44**(8), 1892–1895 (2019)
9. Li, D., Chen, C., Li, J., Yan, Q.: Reconstruction of fluorescence molecular tomography based on graph convolution networks. Journal of Optics **22**(4), 045602 (2020)
10. Lucas, A., Iliadis, M., Molina, R., Katsaggelos, A.K.: Using deep neural networks for inverse problems in imaging: beyond analytical methods. IEEE Signal Processing Magazine **35**(1), 20–36 (2018)
11. Lv, Y., Tian, J., Cong, W., Wang, G., Luo, J., Yang, W., Li, H.: A multilevel adaptive finite element algorithm for bioluminescence tomography. Optics Express **14**(18), 8211–8223 (2006)
12. Markwald, M., Demidova, E.: Refuel: rule extraction for imbalanced neural node classification. Machine Learning **113**(9), 6227–6246 (2024)
13. Monga, V., Li, Y., Eldar, Y.C.: Algorithm unrolling: Interpretable, efficient deep learning for signal and image processing. IEEE Signal Processing Magazine **38**(2), 18–44 (2021)
14. Ntziachristos, V.: Fluorescence molecular imaging. Annu. Rev. Biomed. Eng. **8**(1), 1–33 (2006)
15. Ntziachristos, V., Ripoll, J., Wang, L.V., Weissleder, R.: Looking and listening to light: the evolution of whole-body photonic imaging. Nature biotechnology **23**(3), 313–320 (2005)
16. Schweiger, M., Arridge, S.R., Hiraoka, M., Delpy, D.T.: The finite element method for the propagation of light in scattering media: boundary and source conditions. Medical physics **22**(11), 1779–1792 (1995)
17. Shi, J., Liu, F., Zhang, G., Luo, J., Bai, J.: Enhanced spatial resolution in fluorescence molecular tomography using restarted l1-regularized nonlinear conjugate gradient algorithm. Journal of Biomedical Optics **19**(4), 046018–046018 (2014)
18. Soubret, A., Ripoll, J., Ntziachristos, V.: Accuracy of fluorescent tomography in the presence of heterogeneities: study of the normalized born ratio. IEEE transactions on medical imaging **24**(10), 1377–1386 (2005)
19. Wang, B., Li, S., Zhang, H., Li, J., Zhang, L., Yu, J., He, X., Guo, H.: Deep system prior based graph convolution network for nir-ii fluorescence molecular tomography. Computer Methods and Programs in Biomedicine p. 108948 (2025)
20. Weissleder, R., Nahrendorf, M.: Advancing biomedical imaging. Proceedings of the National Academy of Sciences **112**(47), 14424–14428 (2015)
21. Yang, Y., Sun, J., Li, H., Xu, Z.: Admm-csnet: A deep learning approach for image compressive sensing. IEEE transactions on pattern analysis and machine intelligence **42**(3), 521–538 (2018)
22. Zhang, G., Cao, X., Zhang, B., Liu, F., Luo, J., Bai, J.: Map estimation with structural priors for fluorescence molecular tomography. Physics in medicine and biology **58**(2), 351–372 (2013)
23. Zhang, J., Ghanem, B.: Ista-net: Interpretable optimization-inspired deep network for image compressive sensing. In: Proceedings of the IEEE conference on computer vision and pattern recognition. pp. 1828–1837 (2018)
24. Zhang, P., Fan, G., Xing, T., Song, F., Zhang, G.: Uhr-deepfmt: ultra-high spatial resolution reconstruction of fluorescence molecular tomography based on 3-d fusion dual-sampling deep neural network. IEEE Transactions on Medical Imaging **40**(11), 3217–3228 (2021)
25. Zhang, P., Ma, C., Song, F., Fan, G., Sun, Y., Feng, Y., Ma, X., Liu, F., Zhang, G.: A review of advances in imaging methodology in fluorescence molecular tomography. Physics in Medicine & Biology **67**(10), 10TR01 (2022)

26. Zhao, T., Zhang, X., Wang, S.: Graphsmote: Imbalanced node classification on graphs with graph neural networks. In: Proceedings of the 14th ACM international conference on web search and data mining. pp. 833–841 (2021)